19th International Conference on
Adaptive Structures and Technologies
October 6-9, 2008
Ascona, Switzerland

Gain-Scheduled Control of Smart Link System with Dynamic Characteristic Variation

I. Kajiwara[1*], R. Tsuchiya[2], and S. Ishizuka[3]
[1] Department of Mechanical and Aerospace Engineering, Tokyo Institute of Technology, Japan
[2] Sony Corporation, Japan
[3] Cybernet systems co.,Ltd., Japan
*Corresponding author: 2-12-1 O-okayama, Meguro-ku, Tokyo 152-8552, Japan
Tel : 81(3)5734-2502, Fax: 81(3)5734-2502, E-mail: kajiwara@mech.titech.ac.jp

ABSTRACT

This study is concerned with a vibration control strategy for a flexible-link system to achieve effective vibration suppression. It is required that the control system adapts to the dynamic characteristic variation of the system. A smart-link system composed of piezoelectric actuators and gain-scheduled controller is proposed to cope with change of the variable parameters which causes the dynamic characteristic variation of the system. An adaptive control is conducted by scheduling some LTI controllers to keep the stability and performance against the change of the variable parameters. The appropriate actuator location is determined by the target mode shapes. The scheduling gains for the LTI controllers designed at their operating points are optimized to obtain effective vibration suppression of the system.

Keywords: smart structure, gain-scheduled control, optimization, adaptive control

1. INTRODUCTION

Vibration suppression is very important to improve the performance of mechanical systems. Smart structure using lightweight devices such as piezoelectric sensors and actuators is a key technology to enhance the vibration control performance. Varadarajan (1998) & Saggere (1999) studied shape control of smart structure using piezoelectric materials [1, 2]. Ray (1998) investigated an optimal control of smart structure with piezoelectric sensor and actuator layers [3]. Bailey & Hubbard (1985) proposed simple control algorithm for transient vibration control by constant amplitude actuator and constant gain controller [4]. Crawly & Luis (1987) analyzed the stiffness effect of piezoelectric actuators to the elastic property of host structures [5]. Tzou (1991) investigated the piezoelectric effect on the vibration control through a modal shape analysis [6]. Choi & Lee (1997) proposed a robust force tracking control of a flexible gripper driven by a piezoceramic actuator [7]. Designing piezoelectric modal sensors and modal actuators [8, 9] have been examined for the efficient vibration control by Sun (1999) and Ryou (1998). Benjeddou (1999) presented a mechanism capable of dealing with either extension or shear actuation [10]. Uwe & Lother (1999) investigated an active vibration control of a car body using experimental modal analysis and modal controller [11]. Ono & Kajiwara (2007) investigated an integrated optimization of piezoelectric location and control system to enhance the vibration and acoustic control performance [12]. Almost these researches are related to motion and vibration control with smart structure modeled as a fixed linear time-invariant (LTI) system.

However, the structural dynamic characteristics vary continuously in practical working conditions of mechanical systems. In this case, it is required to construct a control system that adapts to the dynamic characteristic variation of the system. Takagi (1999) & Kajiwara (2001) employed a gain-scheduled controller to cope with the dynamic characteristic variation of the system [13, 14]. It is expected that the enhanced vibration suppression can be achieved by synthesizing the adaptive control strategy and smart structure technology. From this background, this study proposes a gain-scheduled control strategy of smart structures with dynamic characteristic variation in order to achieve desirable vibration suppression.

This study considers vibration suppression of a flexible-link manipulator system which has dynamic characteristic variation. The dynamic characteristics of the system are varied according to variable parameters such as the configuration and holding mass at the tip of the manipulator. In order to adapt to the change of the variable parameters, a smart-link system is constituted by the smart structure technology with piezoelectric actuators and gain-scheduled controller. The piezoelectric actuators are appropriately placed to control the target mode vibration. The structure is modeled by finite element analysis and then the model reduction with the modal coordinate transformation is carried out. The control system is designed by solving the H_2 control problem using a reduced-order modal model. An adaptive control is conducted by scheduling some LTI controllers to keep the stability and performance against the dynamic characteristic variation of the system. The design problem for improving the H_2 performance is defined and then the scheduling gains for their LTI controllers are optimized by SQP algorithm, resulting in an enhanced performance for the vibration control. The performance of the proposed gain-scheduled control system is evaluated by simulation and experiment in this study.

2. CONTROLLED OBJECT AND MODELING

The controlled object with two flexible-links is shown in Fig.1. This system is nonlinear and time-varying with respect to the elbow angle $\boldsymbol{\phi}$ and holding mass $\boldsymbol{m_2}$ at the tip of the manipulator. The variable parameter is defined by

$$\boldsymbol{\theta} = \begin{Bmatrix} \boldsymbol{\phi} \\ \boldsymbol{m}_2 \end{Bmatrix} \tag{1}$$

The linear modeling of this system is carried out at a fixed elbow angle and holding mass as a design point of the variable parameter. This system is modeled by FEM with ANSYS at the design point and transformed into modal coordinate in order to describe a reduced-order state equation which is appropriate for the control system design.

The piezoelectric ceramics and accelerometer are employed as actuator and sensor in the smart structure. The control forces are applied at the both ends of the actuator. An accelerometer is installed to detect the acceleration that is used for a feedback signal in vibration control system. In this study, modeling of the smart structure is carried out with the finite element and modal analyses by which the modeling of arbitrary shape structures and the control system design can be effectively executed [12]. Equation of motion of the structural system is described as

$$\boldsymbol{M}_s(\bar{\boldsymbol{\theta}})\ddot{\boldsymbol{x}} + \boldsymbol{C}_s(\bar{\boldsymbol{\theta}})\dot{\boldsymbol{x}} + \boldsymbol{K}_s(\bar{\boldsymbol{\theta}})\boldsymbol{x} = \boldsymbol{B}_{1s}(\bar{\boldsymbol{\theta}})\boldsymbol{w} + \boldsymbol{B}_{2s}(\bar{\boldsymbol{\theta}})\boldsymbol{u} \tag{2}$$

where $\boldsymbol{M_s}(\bar{\boldsymbol{\theta}})$ and $\boldsymbol{K_s}(\bar{\boldsymbol{\theta}})$ are the mass and stiffness matrices, respectively, and $\boldsymbol{C_s}(\bar{\boldsymbol{\theta}})$ is the assumed proportional viscous damping matrix. $\boldsymbol{x}$, $\boldsymbol{w}$ and $\boldsymbol{u}$ are the displacement, disturbance and control input vectors, respectively. In Eq.(2), $\bar{\boldsymbol{\theta}}$ represents a design point on the elbow angle and holding mass which will be the scheduling parameter in control system. The degree-of-freedom of Eq.(2) becomes generally so large because of using FEM that the control system should not be designed directly to this

spatial model. The coordinate transformation into the modal space is appropriate to conduct the model reduction for control system design. Adopting the lower natural modes $\boldsymbol{\Phi}(\bar{\boldsymbol{\theta}})$, Eq.(2) is transformed to the reduced-order state equation with the transformation $\boldsymbol{x} = \boldsymbol{\Phi}(\bar{\boldsymbol{\theta}})\boldsymbol{\xi}$:

$$\dot{\boldsymbol{q}} = \boldsymbol{A}(\bar{\boldsymbol{\theta}})\boldsymbol{q} + \boldsymbol{B}_1(\bar{\boldsymbol{\theta}})\boldsymbol{w} + \boldsymbol{B}_2(\bar{\boldsymbol{\theta}})\boldsymbol{u} \tag{3}$$

where

$$\boldsymbol{q} = \begin{Bmatrix} \boldsymbol{\xi} \\ \dot{\boldsymbol{\xi}} \end{Bmatrix}, \quad \boldsymbol{A} = \begin{bmatrix} 0 & \boldsymbol{I}_r \\ -\boldsymbol{\Lambda}(\bar{\boldsymbol{\theta}}) & -\boldsymbol{\Phi}(\bar{\boldsymbol{\theta}})^T \boldsymbol{C}_s(\bar{\boldsymbol{\theta}})\boldsymbol{\Phi}(\bar{\boldsymbol{\theta}}) \end{bmatrix}$$

$$\boldsymbol{B}_1 = \begin{bmatrix} 0 \\ \boldsymbol{\Phi}(\bar{\boldsymbol{\theta}})^T \boldsymbol{B}_{1s}(\bar{\boldsymbol{\theta}}) \end{bmatrix}, \quad \boldsymbol{B}_2 = \begin{bmatrix} 0 \\ \boldsymbol{\Phi}(\bar{\boldsymbol{\theta}})^T \boldsymbol{B}_{2s}(\bar{\boldsymbol{\theta}}) \end{bmatrix}$$

$\boldsymbol{\Lambda}(\bar{\boldsymbol{\theta}})$ is the diagonal eigenvalue matrix and the modal matrix $\boldsymbol{\Phi}(\bar{\boldsymbol{\theta}})$ is normalized with the mass matrix. $\boldsymbol{B}_{2s}(\bar{\boldsymbol{\theta}})$ can be determined by the relation between the control input $\boldsymbol{u}$ and the moment caused by the force from the piezoelectric actuator. The force $\boldsymbol{f}$ applied by the piezoelectric actuator is linear for the input voltage and so the relation between the control input $\boldsymbol{u}$ and the force $\boldsymbol{f}$ is described by $\boldsymbol{f} = \boldsymbol{b}_{2s}\boldsymbol{u}$ where $\boldsymbol{b}_{2S}$ is a constant.

The output equation is generally described as

$$\boldsymbol{y}_2 = \boldsymbol{C}_2(\bar{\boldsymbol{\theta}})\boldsymbol{q} + \boldsymbol{D}_{21}(\bar{\boldsymbol{\theta}})\boldsymbol{w} + \boldsymbol{D}_{22}(\bar{\boldsymbol{\theta}})\boldsymbol{u} \tag{4}$$

In this study, structural acceleration is detected by the accelerometer as feedback signal. Accelerometers are suitable to be installed in the smart structures since the external reference is not required for them. In case of the acceleration output, substituting the modal transformation $\boldsymbol{x} = \boldsymbol{\Phi}(\bar{\boldsymbol{\theta}})\boldsymbol{\xi}$ into Eq.(2) yields the modal acceleration:

$$\begin{aligned} \ddot{\boldsymbol{\xi}} = &-\boldsymbol{\Phi}(\bar{\boldsymbol{\theta}})^T \boldsymbol{C}_s(\bar{\boldsymbol{\theta}})\boldsymbol{\Phi}(\bar{\boldsymbol{\theta}})\dot{\boldsymbol{\xi}} - \boldsymbol{\Lambda}(\bar{\boldsymbol{\theta}})\boldsymbol{\xi} + \boldsymbol{\Phi}(\bar{\boldsymbol{\theta}})^T \boldsymbol{B}_{1s}(\bar{\boldsymbol{\theta}})\boldsymbol{w} \\ &+ \boldsymbol{\Phi}(\bar{\boldsymbol{\theta}})^T \boldsymbol{B}_{2s}(\bar{\boldsymbol{\theta}})\boldsymbol{u} \end{aligned} \tag{5}$$

From Eq.(5) and the detected acceleration $\boldsymbol{y}_a = \boldsymbol{C}_a(\bar{\boldsymbol{\theta}})\ddot{\boldsymbol{x}}$, each coefficient matrix in Eq.(4) for the output equation becomes

$$\begin{aligned} \boldsymbol{C}_2 &= \boldsymbol{C}_a(\bar{\boldsymbol{\theta}})\boldsymbol{\Phi}(\bar{\boldsymbol{\theta}})\left[-\boldsymbol{\Lambda}(\bar{\boldsymbol{\theta}}) \quad -\boldsymbol{\Phi}(\bar{\boldsymbol{\theta}})^T \boldsymbol{C}_s(\bar{\boldsymbol{\theta}})\boldsymbol{\Phi}(\bar{\boldsymbol{\theta}})\right] \\ \boldsymbol{D}_{21} &= \boldsymbol{C}_a(\bar{\boldsymbol{\theta}})\left[0 \quad \boldsymbol{\Phi}(\bar{\boldsymbol{\theta}})\right]\boldsymbol{B}_1(\bar{\boldsymbol{\theta}}) \\ \boldsymbol{D}_{22} &= \boldsymbol{C}_a(\bar{\boldsymbol{\theta}})\left[0 \quad \boldsymbol{\Phi}(\bar{\boldsymbol{\theta}})\right]\boldsymbol{B}_2(\bar{\boldsymbol{\theta}}) \end{aligned} \tag{6}$$

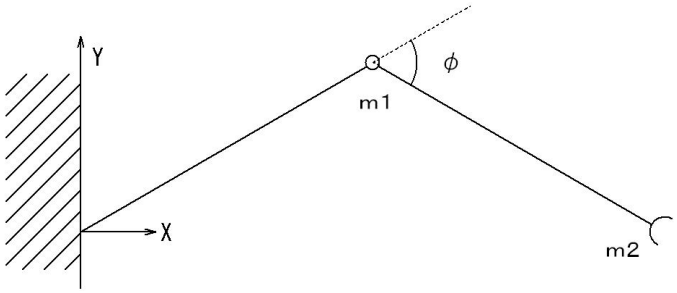

Figure 1. Flexible-link system

3. CONTROL SYSTEM DESIGN

3-1. Controller Design at a Fixed Design Point

The block diagram of the control system for a fixed design point is shown in Fig.2. *P*(*s*) is the

controlled object described by Eqs.(3) and (4), and $K(s)$ is the dynamic compensator to be designed as controller. H_2 control problem is considered in this study. The controller $K(s)$ is obtained by conducting the control problem:

$$\min . \left\| \boldsymbol{T}_{y1w} \right\|_2 \tag{7}$$

where $\boldsymbol{T}_{y1w}$ is the transfer function matrix between the disturbance $\boldsymbol{w}$ and the controlled variable $\boldsymbol{y}_1$. The controlled variable is described as

$$\boldsymbol{y}_1 = \begin{Bmatrix} \boldsymbol{Q}^{1/2} \boldsymbol{z}_1 \\ \boldsymbol{R}^{1/2} \boldsymbol{u} \end{Bmatrix} \tag{8}$$

where $\boldsymbol{z}_1$ is the controlled response, and $\boldsymbol{Q}$ and $\boldsymbol{R}$ are the weighting matrices. The control problem in Eq.(7) is equivalent to

$$\min . \boldsymbol{E}[\boldsymbol{z}_1^T \boldsymbol{Q} \boldsymbol{z}_1 + \boldsymbol{u}^T \boldsymbol{R} \boldsymbol{u}] \tag{9}$$

against a white noise disturbance. In Eq.(9), $E[*]$ shows a mean value. In this study, modal control is considered by defining $\boldsymbol{z}_1$ with modal coordinates.

In the modal control problem, $\boldsymbol{z}_1$ is composed of the modal coordinates and formulated as

$$\boldsymbol{z}_1 = \boldsymbol{W}_{10} \boldsymbol{q} \tag{10}$$

where $\boldsymbol{W}_{10}$ is the modal weighting matrix defined by

$$\boldsymbol{W}_{10} = \boldsymbol{diag}[\boldsymbol{w}_1, \boldsymbol{w}_2, \cdots \boldsymbol{w}_{2r}] \tag{11}$$

r is the number of the adopted modes. Weighting each modal coordinate with each coefficient easily achieves the modal shaping which can mainly suppress the target mode vibration. Frequency weighting functions are generally used for achieving the frequency shaping, however, the order of the controller in this case is increased according to the orders of the frequency weighting functions. The modal control shown here does not increase the order of the controller and so is practically advantageous for developing the real systems.

From Eq.(10), the controlled variable $\boldsymbol{y}_1$ is described as

$$\boldsymbol{y}_1 = \boldsymbol{C}_1 \boldsymbol{q} + \boldsymbol{D}_{12} \boldsymbol{u} \tag{12}$$

where $\boldsymbol{C}_1$ and $\boldsymbol{D}_{12}$ take the form:

$$\boldsymbol{C}_1 = \begin{bmatrix} \boldsymbol{Q}^{1/2} \boldsymbol{W}_{10} \\ 0 \end{bmatrix}$$

$$\boldsymbol{D}_{12} = \begin{bmatrix} 0 \\ \boldsymbol{R}^{1/2} \boldsymbol{I} \end{bmatrix}$$

The optimal control law with the control problem (7) or (9) is obtained as a form of state feedback:

$$\boldsymbol{u} = -\boldsymbol{F} \boldsymbol{q} \tag{13}$$

The optimal feedback gain $\boldsymbol{F}$ is

$$\boldsymbol{F} = -\boldsymbol{R}^{-1} \boldsymbol{B}_2^T \boldsymbol{P} \tag{14}$$

where $\boldsymbol{P}$ is the solution of the Riccati equation:

$$\boldsymbol{A}^T \boldsymbol{P} + \boldsymbol{P} \boldsymbol{A} + \boldsymbol{W}_{10}^T \boldsymbol{Q} \boldsymbol{W}_{10} - \boldsymbol{P} \boldsymbol{B}_2 \boldsymbol{R}^{-1} \boldsymbol{B}_2^T \boldsymbol{P} = 0 \tag{15}$$

Each performance index with respect to the controlled response and the control input is

$$\boldsymbol{H}_{z_1} = \boldsymbol{E}[\boldsymbol{z}_1^T \boldsymbol{z}_1] \quad , \quad \boldsymbol{H}_u = \boldsymbol{E}[\boldsymbol{u}^T \boldsymbol{u}] \tag{16}$$

These performance indices can be calculated by

$$H_{z_1} = trace[C_{10} X C_{10}^T], \quad H_u = trace[F X F^T] \tag{17}$$

where X is the solution of the Lyapunov equation:

$$XG^T + GX + B_1 B_1^T = 0 \tag{18}$$

where $G = A - B_2 F$.

In output feedback system, the output feedback low $u = K(s)y$ is described as state-space form:

$$\begin{aligned} q_K &= A_K q_K + B_K y \\ u &= C_K q_K + D_K y \end{aligned} \tag{19}$$

In Eq.(19), the system matrices A_K, B_K, C_K and D_K of the controller are designed with the LMI solver.

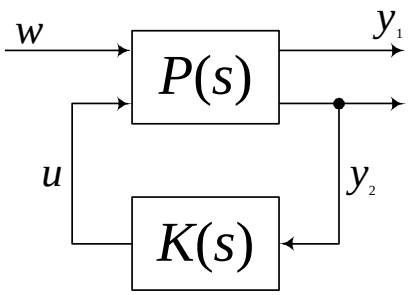

Figure 2. Control system at a fixed design point

3-2. Gain-Scheduled Control System

The LTI controller described in Eq.(19) is available only in the vicinity of the design point $\bar{\theta}$ and does not guarantee the stability of the closed-loop system in wide working area. Therefore, the controller at an optional point is constructed by scheduling some controllers designed at their design points [14]. Each LTI controller is designed at each design point $\{\bar{\theta}_i\}_{i=1}^n$. The optional point θ is expressed by the convex decomposition with the operating points as

$$\begin{aligned} &\theta(t) = \eta_1 \bar{\theta}_1 + \eta_2 \bar{\theta}_2 + \cdots + \eta_n \bar{\theta}_n \\ &\eta_i \geq 0, \ \sum_{i=1}^{n} \eta_i = 1 \end{aligned} \tag{20}$$

The controller to be designed at the point θ is

$$K(s,\theta) := \left[\begin{array}{c|c} A_K(\theta) & B_K(\theta) \\ \hline C_K(\theta) & D_K(\theta) \end{array}\right] \tag{21}$$

When the system is affine to the variable parameter, the gain-scheduled controller is described as

$$\left[\begin{array}{c|c} A_K(\theta) & B_K(\theta) \\ \hline C_K(\theta) & D_K(\theta) \end{array}\right] = \sum_{i=1}^{n} \eta_i \left[\begin{array}{c|c} A_K(\bar{\theta}_i) & B_K(\bar{\theta}_i) \\ \hline C_K(\bar{\theta}_i) & D_K(\bar{\theta}_i) \end{array}\right] \tag{22}$$

where $\eta_i (i = 1, \cdots, n)$ show the scheduling gains. The gain-scheduled controller is constituted by the interpolation of the LTI controllers designed at the design points which are given by

$$K_i := \left[\begin{array}{c|c} A_K(\bar{\theta}_i) & B_K(\bar{\theta}_i) \\ \hline C_K(\bar{\theta}_i) & D_K(\bar{\theta}_i) \end{array}\right] \tag{23}$$

The block diagram of the gain-scheduled control system is shown in Fig.3.

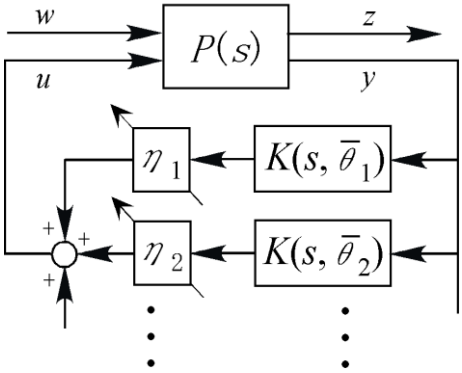

Figure 3. Gain-scheduled control system

4. OPTIMIZATION OF SCHEDULING GAINS

The controlled performance and the stability of the closed-loop system have to be maintained against the change of the variable parameter since the characteristics of the manipulator with multiple links highly depend on its configuration and holding mass. The flexible-link system is not affine with respect to the variable parameter and so the scheduling gains obtained by the convex decomposition in Eq.(20) don't guarantee the closed-loop performance and stability. In this study, the robust stability at an optional point during the motion is guaranteed by conducting an optimization problem.

Describing the design variable on the scheduling gains as $\boldsymbol{\eta}(\boldsymbol{\theta})$, an optimization problem can be defined as

$$\begin{aligned} &\min .: \boldsymbol{J}\left(\boldsymbol{\eta}(\boldsymbol{\theta}), \boldsymbol{\theta}\right) \\ &\text{subj.}: \boldsymbol{g}_{\min} \le \boldsymbol{g}_c \le \boldsymbol{g}_{\max} \end{aligned} \tag{24}$$

where $\boldsymbol{J}(\boldsymbol{\eta}(\boldsymbol{\theta}), \boldsymbol{\theta})$ and $\boldsymbol{g}_c(\boldsymbol{\eta}(\boldsymbol{\theta}), \boldsymbol{\theta})$ are the objective and constraint functions depending on both scheduling gains and design points such as the closed-loop norms described in the control problem (7) and (9). Giving $\boldsymbol{\theta}$ at a design point, the optimal scheduling gains are obtained by solving the optimization problem. $\boldsymbol{\theta}$ is changed in the working area and the optimization problem is conducted at some design points of $\boldsymbol{\theta}$. As a result, the optimal design variable is solved as function of $\boldsymbol{\theta}$.

Reducing $\boldsymbol{H}_{z1}$ in Eq.(16) enhances the vibration control performance. On the other hand, a consumable control cost $\boldsymbol{H}_u$ is limited because of using the piezoelectric actuators in this system and so the maximum control cost should be taken into account in the control system design. A simultaneous optimization problem to reduce the controlled response under the constraints on the control cost $\boldsymbol{H}_u$ is appropriate to achieve the enhanced control performance and can be defined by giving the objective and constraint function in the optimization problem (24) as

$$\boldsymbol{J} = \boldsymbol{H}_{z1} \quad , \quad \boldsymbol{g}_c = \boldsymbol{H}_u \tag{25}$$

The optimization problem (24) is executed by SQP algorithm.

5. SIMULATION AND EXPERIMENT

The elbow angle changes between 0 and 120 degrees and the holding mass changes between 0 and 40 grams. The structural system is modeled with lower 4 natural modes. The constitution of the smart structure is shown in Fig.4 in which three piezoelectric actuators and an accelerometer are installed on the flexible-links. The dimension and property of the flexible-link system are shown in Table 1. The accelerometer is used to detect the acceleration that is used for a feedback signal in vibration control

system. Therefore, this system is three inputs and one output system. The thickness and width of the piezoelectric actuators are 0.5mm and 20mm, respectively, and these actuators are bonded to the link surface by a very thin adhesive layer. The maximum input to the piezoelectric actuator is 150V. The actuators are appropriately placed on the structure to control the vibration of lower 4 natural modes. Another actuator for applying the disturbance force w is bonded on the backside of the 1st link. First, an LTI controller is designed at a given variable parameter, $\theta = (60^\circ, 20g)$. This variable parameter is the center of the working area. And H_2 modal control is employed to reduce the vibration of the lowest 4 natural modes. In order to evaluate the control performance, the control performance factor γ is defined by

$$\gamma = \frac{\|T_{z1w}(j\omega)\|_2}{\|V_{z1w}(j\omega)\|_2} \tag{26}$$

In Eq.(26), $T_{z1w}(j\omega)$ is the transfer function matrix with control between w and z_1, and $V_{z1w}(j\omega)$ is that without control. From this definition, smaller γ means better control performance. Figure 5 shows the relation between γ and θ with the LTI controller. The dark region in Fig.5 is the unstable region of the closed-loop system. Figure 6 shows the region where the control cost H_u exceeds the regulation value H_{uc} at the design point. The control performance factors and control costs were calculated with 1648 closed-loop systems to obtain Figs.5 and 6 by dividing the working range of both scheduling parameters into 41 points. From Figs.5 and 6, the designed LTI controller is not available in the whole working area of the system.

Table 1. Dimension and property of manipulator

Arm length(mm)	90
Arm width(mm)	20
Arm thickness(mm)	1
Material	Steel
Young's modulus(GPa)	2.06×10^{11}
Poisson's ratio	0.3
Density (kg/m^3)	7.86×10^3
Joint angle ϕ (deg)	0～120
Joint mass m_1 (g)	15
Additional mass m_2(g)	0～40

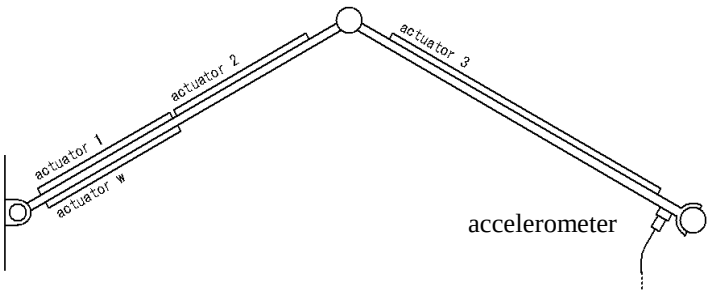

Figure 4. Smart-link system

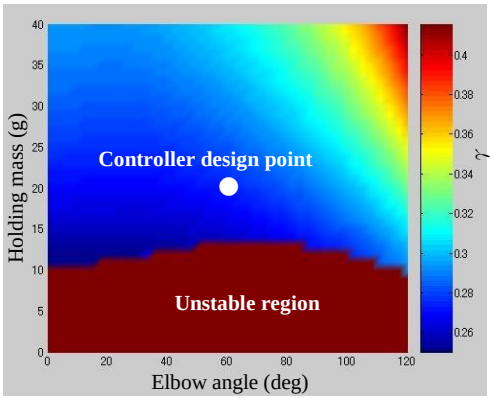

Figure 5. Relation between γ and θ with an LTI controller

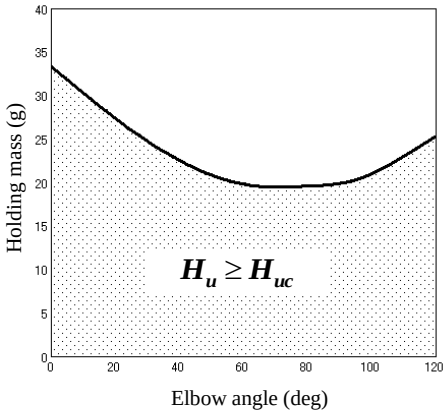

Figure 6. Region where control cost exceeds that at the design point

Next, the gain-scheduled control is employed for improving the closed-loop performance and stability of the system. The new design points are added at the four corners of the variable parameters. The total number of the design points becomes five. These design points of the variable parameter are given by

1) $\boldsymbol{\theta}_1 = (0,0)^T$: Controller $\boldsymbol{K_{00000}}$
2) $\boldsymbol{\theta}_2 = (120,0)^T$: Controller $\boldsymbol{K_{12000}}$
3) $\boldsymbol{\theta}_3 = (60,20)^T$: Controller $\boldsymbol{K_{06020}}$
4) $\boldsymbol{\theta}_4 = (0,40)^T$: Controller $\boldsymbol{K_{00040}}$
5) $\boldsymbol{\theta}_5 = (120,40)^T$: Controller $\boldsymbol{K_{12040}}$

Figure 7 shows a schematic diagram of these design points. In Fig.7, the four triangle regions constituted by the three design points are defined for constructing the gain-scheduled control system. The gain-scheduled control system is composed of the three LTI controllers designed at their design points and scheduling gains in each region. The control law is described as

$$\boldsymbol{u} = \begin{cases} (\eta_1 \boldsymbol{K}_{06020} + \eta_2 \boldsymbol{K}_{00000} + \eta_3 \boldsymbol{K}_{00040})\boldsymbol{y}_2 & (\textbf{region I}) \\ (\eta_1 \boldsymbol{K}_{06020} + \eta_2 \boldsymbol{K}_{00040} + \eta_3 \boldsymbol{K}_{12040})\boldsymbol{y}_2 & (\textbf{region II}) \\ (\eta_1 \boldsymbol{K}_{06020} + \eta_2 \boldsymbol{K}_{12040} + \eta_3 \boldsymbol{K}_{12000})\boldsymbol{y}_2 & (\textbf{region III}) \\ (\eta_1 \boldsymbol{K}_{06020} + \eta_2 \boldsymbol{K}_{12000} + \eta_3 \boldsymbol{K}_{00000})\boldsymbol{y}_2 & (\textbf{region IV}) \end{cases} \tag{27}$$

where $\eta_i (i = 1,2,3)$ show the scheduling gains. The optimal scheduling gains are obtained by solving the optimization problem:

$$\begin{aligned} &\min .: \boldsymbol{H}_{z1} \\ &\text{subj.} : \begin{cases} \boldsymbol{H}_u \leq 4.0 \\ 0 \leq \eta_1, \eta_2, \eta_3 \end{cases} \end{aligned} \tag{28}$$

The obtained optimal scheduling gains are shown in Fig.8 as gradation corresponding to their values. Figure 9 shows the relation between γ and θ with the optimal gain-scheduled control. On the other hand, the same relation with the linear gain-scheduled control constituted by the linear interpolation of the three apex LTI controllers in each region is shown in Fig.10. Figure 9 demonstrates an enhanced vibration control performance with the optimal gain-scheduled control over the linear gain-scheduled control in Fig.10. It is also confirmed from Figs.5 and 9 that the control performance and the stability of the closed-loop system have been improved by the optimal gain-scheduled control.

Figure 11 shows the ratio of the control factors with the optimal gain-scheduled control and the optimal control designed for a given variable parameter. From Fig.11, the H_2 norm of the controlled response with the optimal gain-scheduled control is almost equal to that with the optimal control designed for a given variable parameter in the whole working area. The control cost $\boldsymbol{H}_u$ with the optimal gain-scheduled control is nearly equal to the upper bound given by the optimization problem (28) in the whole working area. In actual control system, the controller has the optimal scheduling gain information in Fig.8 as a gain-map table and the real-time control is conducted by taking the optimal scheduling gains according to the variable parameter.

An experiment has been carried out to verify the obtained results. The variable parameter is given by $\boldsymbol{\theta} = (60°, 35\mathbf{g})^T$. The given elbow angle is considered to be a command input. The principal purpose of this experiment is to evaluate the vibration control performance at the final stage of the positioning. This condition belongs to the region II in Fig.7 and so the gain-scheduled controller is composed of $\boldsymbol{K}_{06020}$, $\boldsymbol{K}_{00040}$ and $\boldsymbol{K}_{12040}$. The frequency responses at the tip of the smart-link system are shown in Figs.12 and 13 obtained by simulation and experiment, respectively. Figure 12 shows the ratio of the tip acceleration to the disturbance moment input. On the other hand, Fig.13 shows the ratio of the accelerometer output voltage to the disturbance input voltage. In Figs.12 and 13, the broken line shows the response without control and the solid line with control. There is some error between the calculated and measured resonance/anti-resonance frequencies. It is considered that this error is caused by the difference of the connecting condition of each link and boundary condition between the simulation model and experimental set-up. It is confirmed from the experimental result shown in Fig.13 that the 11dB reduction for the 1st resonance peak, 10dB reduction for the 2nd resonance peak, 15dB reduction for the 3rd resonance peak and 9dB reduction for the 4th resonance peak have been achieved with the optimal gain-scheduled control even though the experimental result is a bit inferior to the analytical result in Fig.12.

The effective vibration suppression is confirmed also in cases of other variable parameters. Moreover, the control performance with the optimal scheduling gains is compared to that with the linear scheduling gains for the other variable parameters, resulting in a superior control performance with the proposed method. It is also interesting to evaluate the vibration control performance during the motion. An experiment to evaluate this property has not been conducted yet, but reducing the vibration at the final stage of the positioning and keeping the stability during the motion are very important and the closed-loop stability is guaranteed by the proposed control system. The evaluation of the vibration suppression during the motion is a future task of this study. It has been verified by this application that the vibration control performance and stability of the flexible-link system with characteristic variation can be enhanced by the proposed smart-link mechanism and gain-scheduled control strategy.

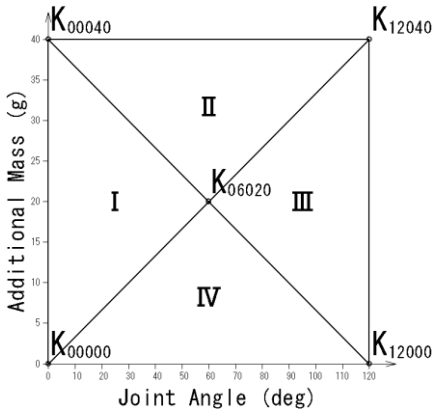

Figure 7. Design points of LTI controllers

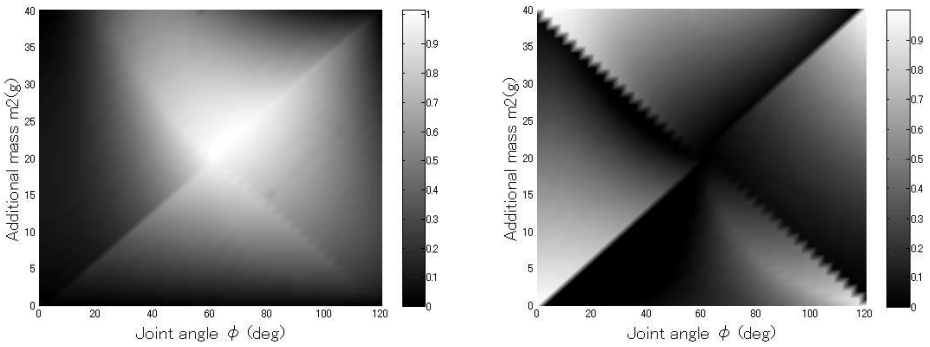

(a) η_1 (b) η_2

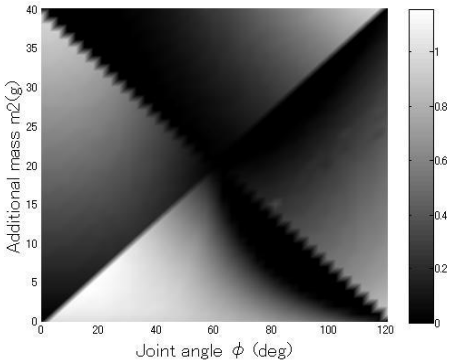

(c) η_3

Figure 8. Optimal scheduling gains

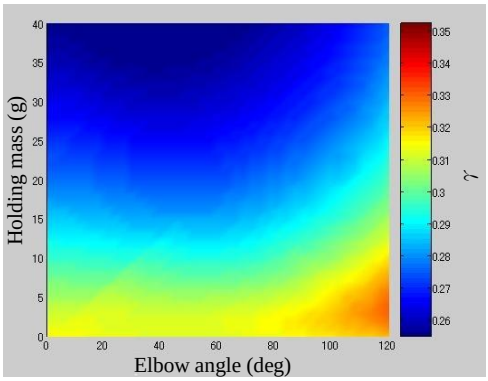

Figure 9. Relation between γ and θ with optimal gain-scheduled control

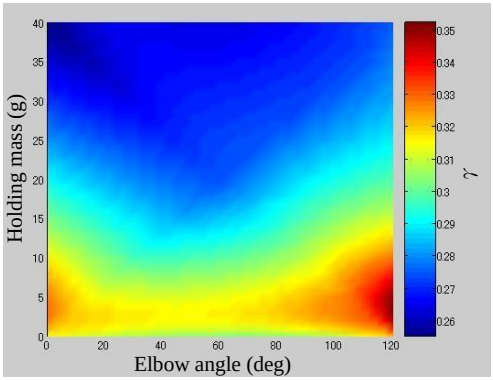

Figure 10. Relation between γ and θ with linear gain-scheduled control

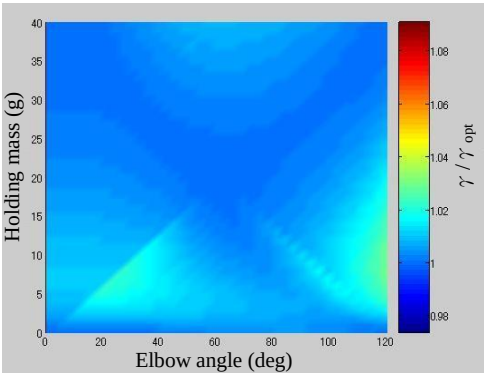

Figure 11. Ratio of control performance factors with the optimal gain-scheduled control and the optimal control

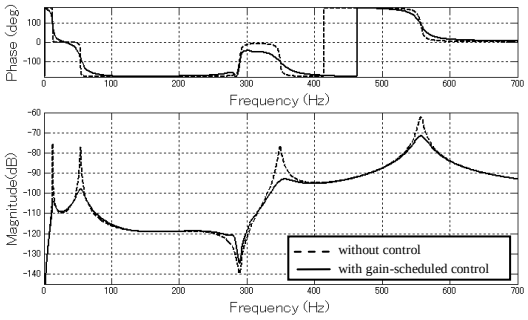

Figure 12. Calculated FRF of smart-link system

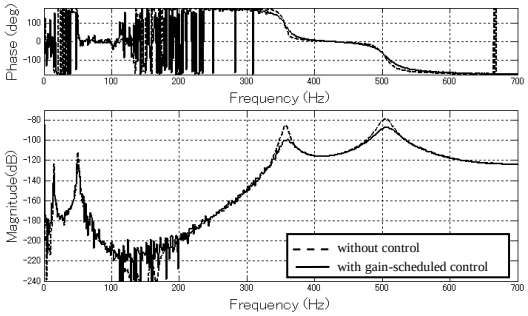

Figure 13. Measured FRF of smart-link system

6. CONCLUSIONS

This study has proposed a vibration control strategy using smart structure technology for a flexible-link system with dynamic characteristic variation. The gain-scheduled controller is employed to cope with the dynamic characteristic variation of the smart-link system. The control system is composed of the multiple LTI controllers designed by H_2 control problem and their scheduling gains. The optimization method of the scheduling gains has also been proposed in order to enhance the vibration control performance satisfying the stability during the motion of the system. The simulation and experiment have been carried out with the 2-link smart manipulator. It has been verified by this study that the enhanced vibration suppression can be achieved by the proposed smart-link mechanism and the gain-scheduled control strategy.

REFERENCES

1. Varadarajan, S., Chandrashekhara, K. and Agarwal, S., Adaptive Shape Control of Laminated Composite Plates Using Piezoelectric Materials, *AIAA Journal*, Vol. 36, No. 9 (1998), pp. 1694-1698.
2. Saggere, L. and Kota, S., Static Shape Control of Smart Structures Using Compliant Mechanisms, *AIAA Journal*, Vol. 37, No. 5 (1999), pp. 572-578.
3. Ray, M. C., Optimal Control of Laminated Plate with Piezoelectric Sensor and Actuator Layers, *AIAA Journal*, Vol. 36, No. 12 (1998), pp. 2204-2208.
4. Bailey, T. and Hubbard, J. E. Jr., Distributed Piezoelectric-Polymer Active Vibration Control of a Cantilever Beam, *Journal of Guidance, Control, and Dynamics*, Vol. 8, No. 5 (1985), pp. 605-611.

5. Crawly, E. F. and de Luis, Use of Piezoelectric Actuators as Elements of Intelligent Structures, *AIAA Journal*, Vol. 25, No. 10 (1987), pp. 1373-1385.
6. Tzou, H. S., Distributed Modal Identification and Vibration Control of Continua: Theory and Applications, *Trans. ASME, Journal of Dynamic Systems, Measurement, and Control*, Vol. 113 (1991), pp. 494-499.
7. Choi, S. and Lee, C., Force Tracking Control of a Flexible Gripper Driven by Piezoceramic Actuators, *Trans. ASME, Journal of Dynamic Systems, Measurement, and Control*, Vol. 119 (1997), pp. 439-446.
8. Sun, D., Wang, D., Xu, Z. L. and Wu, H., Distributed Piezoelectric Element Method for Vibration Control of Smart Plates, *AIAA Journal*, Vol. 37, No. 11 (1999), pp. 1459-1463.
9. Ryou, J., Park, K. and Kim, S., Electrode Pattern Design of Piezoelectric Sensors and Actuators Using Genetic Algorithms, *AIAA Journal*, Vol. 36, No. 2 (1998), pp. 227-233.
10. Benjeddou, A., Trindade, M. A. and Ohayon, R., New Shear Actuated Smart Structure Beam Finite Element, *AIAA Journal*, Vol. 37, No. 3 (1999), pp. 378-383.
11. Uwe S. and Lothar G., Active Vibration Control of a Car Body Based on Experimentally Evaluated Modal Parameters, *Mechanical Systems and Signal Processing*, Vol. 15, No. 1 (1999), pp. 173-188.
12. Ono, K., Kajiwara, I. and Ishizuka, S., Piezoelectric and Control Optimization of Smart Structures for Vibration and Sound Suppression, *International Journal of Vehicle Design*, Vol. 43, Nos. 1-4 (2007), pp. 184-199.
13. Takagi, K. and Nishimura, H., Gain-scheduled Control of a Tower Crane Considering Varying Load-Rope Length, *JSME International Journal, Series C*, Vol. 42, No. 4 (1999), pp.914- 921.
14. Kajiwara, I., Yambe, K. and Nishidome, C., A Control Method for Non-Linear Time-Varying System Using Mixed H_2/H_∞ Control: Position and Force Control of 2-Link Manipulator, *Proceedings of 2001 ASME Design Engineering Technical Conference*, (2001), CD-ROM(No. VIB-21326).